Theoretical physics.
Theory of condensed matter

UDC 538.9

EDN DNZGSD
https://www.doi.org/10.33910/2687-153X-2025-6-1-35-48

Numerical simulations of Gaussian white noise and field-induced phase transition in bulk antiferroelectrics using parameters of ammonium dihydrogen phosphate

S.-Ch. Lim ✉[1]

[1] School of Physics, Universiti Sains Malaysia, 11800 USM, Penang, Malaysia

Author

Siew-Choo Lim, ORCID: 0000-0001-8397-0886, e-mail: sclim@usm.my

For citation: Lim, S.-Ch. (2025) Numerical simulations of Gaussian white noise and field-induced phase transition in bulk antiferroelectrics using parameters of ammonium dihydrogen phosphate. *Physics of Complex Systems*, 6 (1), 35–48. https://www.doi.org/10.33910/2687-153X-2025-6-1-35-48 EDN DNZGSD

Received 24 September 2024; reviewed 27 December 2024; accepted 27 December 2024.

Funding: The study did not receive any external funding.

Abstract. This paper presents phenomenological and numerical studies of Gaussian white noise and field-induced dynamical phase transitions in bulk antiferroelectrics (AFE), focusing on the delayed transition from AFE to ferroelectric (FE) states. The steady states of the AFE are formulated by applying the calculus of variations to the AFE thermodynamic potential, in the absense of external noise. Stochastic relaxation equations for the AFE are then derived using the Landau — Khalatnikov equation, where the AFE thermodynamic potential accounts for both Gaussian white noise and a sinusoidal time-dependent electric field. These equations are solved numerically using the stochastic fourth-order Runge — Kutta (SRK4) method. The results indicate that, for an applied field amplitude of 97% of the transition amplitude, additional Gaussian white noise with amplitudes < 8% of the applied field induces delayed AFE to FE phase transitions, with the time delay inversely proportional to the noise amplitudes.

Keywords: Gaussian white noise, stochastic fourth-order Runge — Kutta (SRK4) method, dynamical phase transition, antiferroelectrics, ferroelectrics

Introduction

Phase transitions in antiferroelectric (AFE) materials are typically characterized by a unique electric polarization that reverses direction at a critical temperature or applied electric field. Below the critical temperature, the AFE to ferroelectric (FE) phase transition occurs when both static and time-dependent electric fields increase beyond their respective critical thresholds. At various static field values, steady states of the AFE systems can be identified. These states exhibit hysteresis patterns in 2D plots of induced polarization versus applied static field. By observing these hysteresis patterns, the system's AFE and FE states can be distinguished. For time-dependent applied electric fields, sinusoidal or other periodic behaviors lead to what is called a dynamic field-induced phase transition, where the dynamic field can drive the system from one phase to another, typically from AFE to FE phases. These phase transitions manifest as abrupt changes in hysteresis patterns, shifting from AFE double hysteresis loops to FE single hysteresis loops (Lines, Glass 1977; Tolédano, Guennou 2016; Zhang et al. 2020; 2023).

In dynamic field-induced phase transitions, the effects of noise are inevitable. Sources of this noise may arise from fluctuating environmental conditions, non-ideal equipment, material degradation (such as aging), electrical interference, thermal fluctuations, imperfect control systems, and other random

disturbances (Garcia-Ojalvo, Sancho 1999; Gardiner 1985; Henkel, Pleimling 2010). Initially, stochastic effects on dynamical phase transitions were used to explain climatic transitions between ice ages and interglacials (Alexandrov et al. 2018; Benzi et al. 1981; Nicolis 1982). The theoretical study of noise-induced phase transitions has gained momentum in other physical systems. For example, in the cubic lattice model (Van den Broeck et al. 1994), spatially extended systems (Cao et al. 2007; Carrillo et al. 2003), and delayed triple-well potential systems (Jin, Xu 2020), among others. Stochastic transitions have also garnered significant interest in quantum systems, such as the system-reservoir model (Ghosh et al. 2005), mesoscopic metal rings (Tong, Vojta 2006), electronic Mach-Zehnder interferometers (Levkivskyi, Sukhorukov 2009), two-dimensional open quantum systems (Dagvadorj et al. 2015), quantum dots (Zhang et al. 2017), and hybrid quantum circuits (Liu et al. 2024), etc.

In this paper, we investigate both phenomenologically and numerically the effects of additional Gaussian white noise on field-induced delayed AFE to FE phase transitions in bulk AFE systems, such as ammonium dihydrogen phosphate (ADP). We first explore how electric fields, both static and time-dependent, influence these phase transitions, with particular attention to hysteresis patterns that help distinguish between AFE and FE states. We further examine the impact of Gaussian white noise on dynamic field-induced AFE to FE phase transitions by evaluating how the frequency and amplitude of the applied electric field, as well as the noise amplitude, affect hysteresis patterns, time series curves, and the delay of phase transition onset.

The study is divided into three parts. In the first part, the steady states of the AFE system are formulated using the bulk AFE thermodynamic potential with an applied static electric field, excluding noise (Lines, Glass 1977; Lim 2022). The resulting equations of state are solved numerically using a root-finding method (Press et al. 1996), and the results are presented graphically in 2D plots. These results serve as a baseline for distinguishing between the AFE and FE phases in the second and third parts of this paper.

In the second part, the adopted AFE thermodynamic potential incorporates Gaussian white noise and a sinusoidal time-dependent electric field. The nonlinear stochastic relaxation equations of the AFE system are formulated by applying the Landau — Khalatnikov equation to this thermodynamic potential. To numerically solve these nonlinear stochastic relaxation equations, we adopt the stochastic fourth-order Runge — Kutta (SRK4) method (Khodabin, Rostami 2015). In the numerical simulations, two sets of frequency and amplitude of the applied field are selected, with the selected amplitudes being smaller than the transition amplitudes without noise. For each set of frequency and amplitude, three sets of numerical data are generated to account for three different noise amplitudes. Specifically, the first two sets correspond to noise amplitudes below the critical value, while the third set corresponds to the critical noise amplitude. The generated data are plotted as time series and hysteresis curves. The abrupt changes in values and the patterns of the curves enable the identification of the transition from AFE to FE phases of the system.

The third part is an extension of the second part, using the same formalism and numerical scheme. The selected frequencies are the same as the frequencies chosen in the second part, but the selected field amplitudes are significantly greater than the transition amplitudes without noise. Two sets of numerical data are generated using the same SRK4 method to account for two moderate noise amplitudes. The generated data are plotted as time series and hysteresis curves, serving as a comparison with the results from the second part.

Part I. AFE and FE steady states in applied static fields

Before applying noise, it is necessary to identify the steady states of the system under a static applied field. The formalism is based on the Landau theory of first-order antiferroelectricity, adopted from previous work (Lim 2022), in which the dimensionless bulk AFE thermodynamic potential is presented in equation (1):

$$g_A = (\psi + t)\, q^2 + t r^2 - (q^4 + 6q^2 r^2 + r^4) + \\ + (q^6 + 15q^4 r^2 + 15q^2 r^4 + r^6) - \bar{e} q\,. \quad (1)$$

g_A, t, $\bar{e}$, q, r, and ψ, are reduced variables, or dimensionless quantities, corresponding to the thermodynamic potential of the AFE system, temperature, applied static electric field, normal electric displacement, staggered electric displacement, and the interaction constant of the AFE sublattices (Lim 2022; Lines,

 https://www.doi.org/10.33910/2687-153X-2025-6-1-35-48

Glass 1977). When the system is in equilibrium, the variation of g_A in equation (1) with respects to q and r is minimized, which gives the equations of state for the AFE system, as shown in equations (2):

$$2(\psi + t)q - (4q^3 + 12qr^2) + (6q^5 + 60q^3r^2 + 30qr^4) - \bar{e} = 0, \tag{2a}$$

$$2tr - (12q^2r + 4r^3) + (30q^4r + 60q^2r^3 + 6r^5) = 0. \tag{2b}$$

From equation (2b), the possible values of r are:

$$r_{FE} = 0, \tag{3a}$$

which corresponds to the field-induced FE phase, and

$$r_{\pm}^2 = \frac{-(15q^2 - 1) \pm \sqrt{180q^4 - 12q^2 + 1 - 3t}}{3}, \tag{3b}$$

which corresponds to the remnant AFE phase under the influence of the applied static field. The existence of the AFE phase is confirmed when the value of $r = r_{\pm}$ is non-zero and real. Substituting equations (3) into equation (2a) gives the equations of state of the AFE system in terms of q versus $\bar{e}$.

To reveal some features of the equations of state, equations (2) and (3) are solved numerically (Press et al. 1996), and the generated data are presented graphically. In the numerical calculations, the material parameters for ammonium dihydrogen phosphate (ADP) are adopted from previous work (Lim 2022). For ADP, the Curie temperature is T_C = 148 K. The fitting of ADP material constants yields $\psi \approx 0.01233$, $t \approx -3.346 \times 10^{-3}$, $e_C \approx 0.41658$, and $f_0 \approx 0.021336524$ at T = 80 K (Lim 2022), where f_0 is the natural frequency of the AFE system. The calculated points for ADP's equations of state are shown in Figure 1.

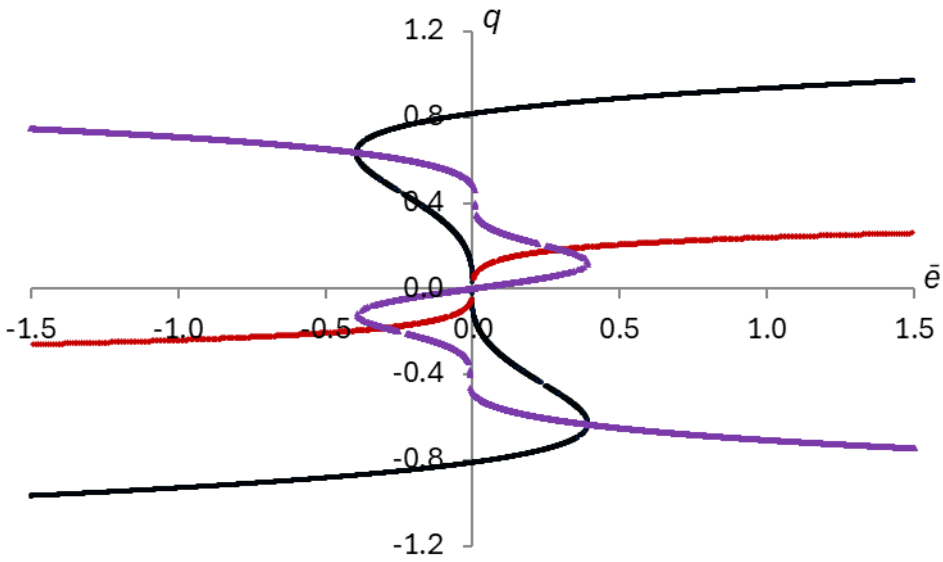

Fig. 1. Steady states for ADP at T = 80 K ($t \approx -3.346 \times 10^{-3}$), where FE states are represented by black dots (r = 0), AFE states by purple dots ($r = r_+$), and red dots ($r = r_-$)

In Figure 1, the black dots, calculated from equations (2a) and (3a), correspond to the field-induced FE states of the system, whereas the red ($r = r_-$) and purple ($r = r_+$) dots, obtained from equations (2a) and (3b), correspond to the remnant AFE states of the system. In Figure 1, the numerical points indicate the existence of AFE states for both $|\bar{e}| < e_C$ and $|\bar{e}| \geq e_C$. However, the bulk AFE system considered here does not account for stress, strain, size, or surface effects that may pin the AFE states for $|\bar{e}| \geq e_C$. Therefore, the condition for the existence of the AFE phase is that the magnitude of the applied static field must be smaller than the coercive field, i. e., $|\bar{e}| < e_C$. To satisfy this condition, the purple and red dots with $|\bar{e}| \geq e_C$

are removed. Additionally, in Figure 1, the AFE and FE states corresponding to the dots with negative slope trends are unstable and are unlikely to exist under an applied static electric field. To retain only the stable and metastable states, points exhibiting negative slopes are also removed (Line, Glass 1977). The results of discarding the unstable states and the AFE states with $|\bar{e}| \geq e_C$ are shown in Figure 2.

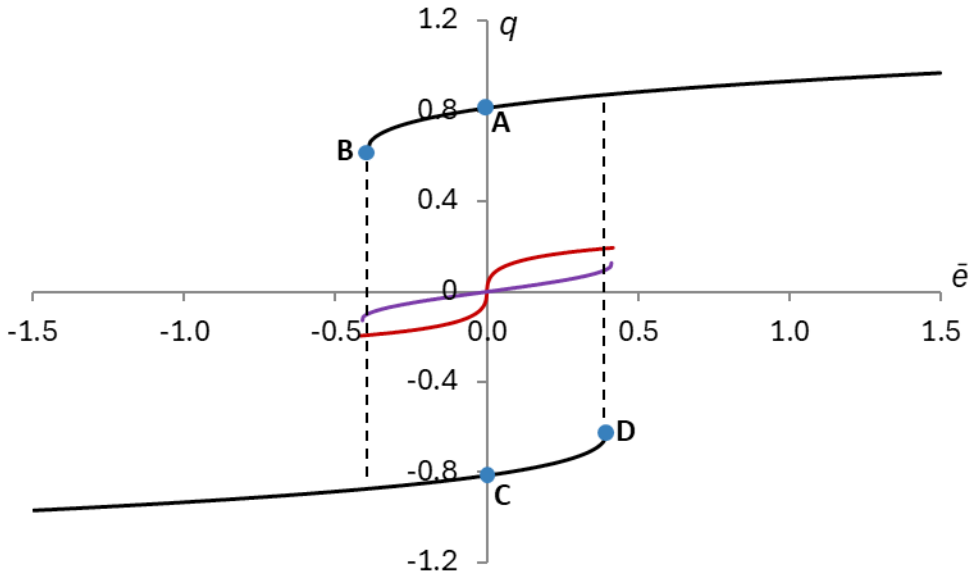

Fig. 2. Metastable states (AB and CD) and stable states of ADP at $T = 80\ K$ ($t \approx -3.346 \times 10^{-3}$), where FE states are represented by black curves ($r = 0$), AFE states by purple curves ($r = r_+$), and red curves ($r = r_-$)

The curves in Figure 2 show obvious hysteresis patterns with discontinuities around $\pm e_C$ for both FE and AFE states. Key differences between FE and AFE states include: (i) the FE states show a single hysteresis pattern, whereas the AFE states show a double hysteresis pattern; (ii) the magnitudes of the normal electric displacement in AFE states (i. e., $|q| < 0.2$) are significantly smaller than those in FE states (i. e., $|q| > 0.6$); (iii) the magnitude of the applied field required to induce discontinuous switching in FE states (i. e., $|\bar{e}| \approx 0.39325 \approx 0.944 e_C$) is smaller than that required in AFE states (i. e., $|\bar{e}| \approx e_C$); and (iv) the FE curves exhibit metastable state curves AB and CD (Line, Glass 1977).

Part II. AFE to FE phase transitions under the influence of applied sinusoidal fields and Gaussian white noise

In the formulation, the applied dynamic fields consist of two components: one is a deterministic sinusoidal field, and the other resembles Gaussian white noise with zero mean, adjustable amplitude, and variance. With these dynamic fields, the dimensionless bulk AFE thermodynamic potential is given in equation (4) (Lim 2022; Van den Broeck et al. 1994):

$$g_A = (\psi + t)q^2 + tr^2 - \left(q^4 + 6q^2r^2 + r^4\right) + \left(q^6 + 15q^4r^2 + 15q^2r^4 + r^6\right) - \\ -eq - D\xi(s)q, \tag{4}$$

where s is the dimensionless time variable, $e = e_0 \sin(2\pi fs)$ is the ***time-dependent applied electric field*** (in what follows referred to as '***field***' or '***applied field***'), and e_0 is the field amplitude. $\xi(s)$ represents Gaussian white noise, and $\mathcal{D} = \sigma e_0$ is the adjustable amplitude of the noise, where σ is a constant. In the presence of the field and noise, the dimensionless Landau — Khalatnikov equation of motion is given by equation (5) (Lim 2022):

$$\frac{d^2x_i}{ds^2} + \gamma\frac{dx_i}{d\tau} = -\frac{\delta g_A}{\delta x_i}, \tag{5}$$

 https://www.doi.org/10.33910/2687-153X-2025-6-1-35-48

where γ is dimensionless damping constant, and x_i represents the dimensionless normal or staggered electric displacements, q and r. The first and second terms in equation (5) represent the acceleration and damping of x_i. $\frac{\delta g_A}{\delta x_i}$ is the variation of g_A in equation (4) with respect to x_i. For small damping, the dynamics of q and r are oscillatory, which has been used to simulate chaotic dynamics without noise in previous works (Lim 2022; 2023). For large damping, such as γ = 1, the first-order time derivative terms dominate, and equation (5) can be approximated as nonlinear first-order stochastic relaxation equations for the AFE system, as shown in equations (6) (Khodabin, Rostami 2015; Van den Broeck et al. 1994):

$$dq = C_q ds + D dw, \tag{6a}$$

$$dr = C_r ds, \tag{6b}$$

where

$$C_q = -2(\psi + t)q + 4\left(q^3 + 3qr^2\right) - 6\left(q^5 + 10q^3r^2 + 5qr^4\right) + e, \tag{7a}$$

$$C_r = -2tr + 4\left(3q^2r + r^3\right) - 6\left(5q^4r + 10q^2r^3 + r^5\right), \tag{7b}$$

$$dw = \xi(s)ds. \tag{7c}$$

Equations (6) are used to simulate the dynamic phase transitions and hysteresis effects of AFE systems. The stochastic fourth-order Runge — Kutta (SRK4) method, an extension of the classic fourth-order Runge — Kutta method (Khodabin, Rostami 2015), is adopted to simulate equations (6). In the numerical scheme, equations (6) are rewritten in vector form, as shown in equation (8):

$$dX_s = C\left(X_s, s\right)ds + D\left(X_s, s\right)dW_s. \tag{8}$$

To solve equation (8), the SRK4 method involves discretizing the time interval into steps and updating the solution iteratively. Let X_n denote the approximation of X_{S_n} at time s_n, and let $\Delta s = s_{n+1} - s_n$. The SRK4 method updates X_{n+1} using the computed intermediate values as shown in equation (9):

$$K_1 = C\left(X_n, s_n\right)\Delta s + D\left(X_n, s_n\right)\Delta W_{n,1}, \tag{9a}$$

$$K_2 = C\left(X_n + \frac{1}{2}K_1, s_n + \frac{1}{2}\Delta s\right)\Delta s + D\left(X_n + \frac{1}{2}K_1, s_n + \frac{1}{2}\Delta s\right)\Delta W_{n,2}, \tag{9b}$$

$$K_3 = C\left(X_n + \frac{1}{2}K_2, s_n + \frac{1}{2}\Delta s\right)\Delta s + D\left(X_n + \frac{1}{2}K_2, s_n + \frac{1}{2}\Delta s\right)\Delta W_{n,3}, \tag{9c}$$

$$K_4 = C\left(X_n + K_3, s_n + \Delta s\right)\Delta s + D\left(X_n + K_3, s_n + \Delta s\right)\Delta W_{n,4}, \tag{9d}$$

where all the terms $\mathcal{D}$ (…, …) in equations (9) are adjustable constants. $\Delta W_{n,1}$, $\Delta W_{n,2}$, $\Delta W_{n,3}$, and $\Delta W_{n,4}$ are independent amplitude increments of the stochastic process with zero mean and variance Δs, i. e., $\Delta W_n \sim \mathcal{N}(0, \Delta s) = \sqrt{\Delta s}\,\mathcal{N}(0,1)$, where $\mathcal{N}(0,1)$ is the Gaussian random variable with zero mean and variance one. The updated solution is given by equation (10):

$$X_{n+1} = X_n + \frac{1}{6}\left(K_1 + 2K_2 + 2K_3 + K_4\right). \tag{10}$$

The material parameters adopted in the simulations are based on the parameters of ADP at $T = 80K$, which are the same as those used to generate Figures 1 and 2.

Before applying Gaussian white noise, two frequencies of the field are selected: $f_1 = 0.5f_0$ and $f_2 = 1.5f_0$. The corresponding transition amplitudes of the field needed to switch the system from AFE hysteresis to FE hysteresis are approximately $e_{0T1} = 1.0162e_C$ and $e_{0T2} = 1.0775e_C$, respectively. To reveal the effects of Gaussian white noise and maintain the periodicity of the induced normal electric displacement as the

applied field, the selected field amplitudes for the two frequencies are $e_{01} = 0.9857e_C$ and $e_{02} = 1.0443e_C$, which are approximately 97% of the corresponding transition amplitudes. The numerical results for the first set of frequency and amplitude, namely $f = f_1 = 0.5f_0$ and $|e_1| = e_{01} = 0.9857e_C$, with a standard deviation of $\sqrt{\Delta s_1} \approx 7.654083178069687 \times 10^{-2}$, are shown in Figures 3 and 4.

In Figure 3, the time series curves are presented as e_1 versus s (i. e., (s, e_1)), along with three q versus s curves (i. e., (s, q_1), (s, q_2), (s, q_3)), and three r versus s curves (i. e., (s, r_1), (s, r_2), (s, r_3)). These curves correspond to three amplitudes of noise: $\mathcal{D}_1 = 0.0630e_{01} = 0.06203610e_C$, $\mathcal{D}_2 = 0.0792e_{01} = 0.07798824e_C$, and $\mathcal{D}_3 = 0.0793e_{01} = 0.07808671e_C$. For all these curves, e_1 is switched on from the 1st to 45th cycles and switched off after the 45th cycle, whereas noise is switched on from the 1st to the 35th cycles, and switched off after the 35th cycle.

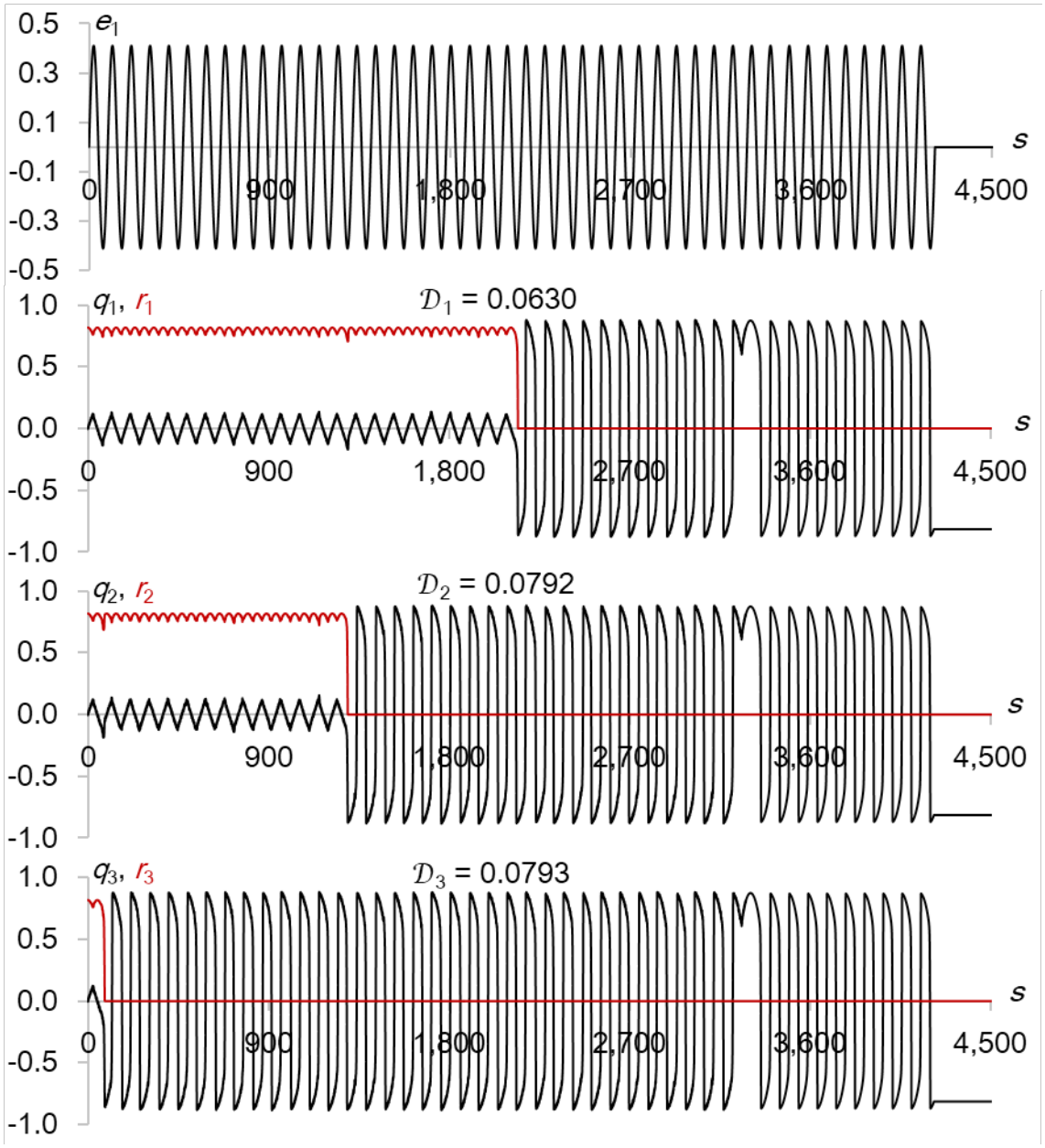

Fig. 3. Time series curves for (s, e_1), (s, q_1), (s, r_1), (s, q_2), (s, r_2), (s, q_3), and (s, r_3) for the 1st to 45th cycles. The three black (s, q) curves and three red (s, r) curves correspond to three amplitudes of noise: $\mathcal{D}_1 = 0.0630e_{01}$, $\mathcal{D}_2 = 0.0792e_{01}$, and $\mathcal{D}_3 = 0.0793e_{01}$. Here, $|e_1| = e_{01} = 0.9857e_C$, $f = f_1 = 0.5f_0$, and $\sqrt{\Delta s_1} \approx 7.654083178069687 \times 10^{-2}$; all noise is switched off after the 35th cycle

https://www.doi.org/10.33910/2687-153X-2025-6-1-35-48

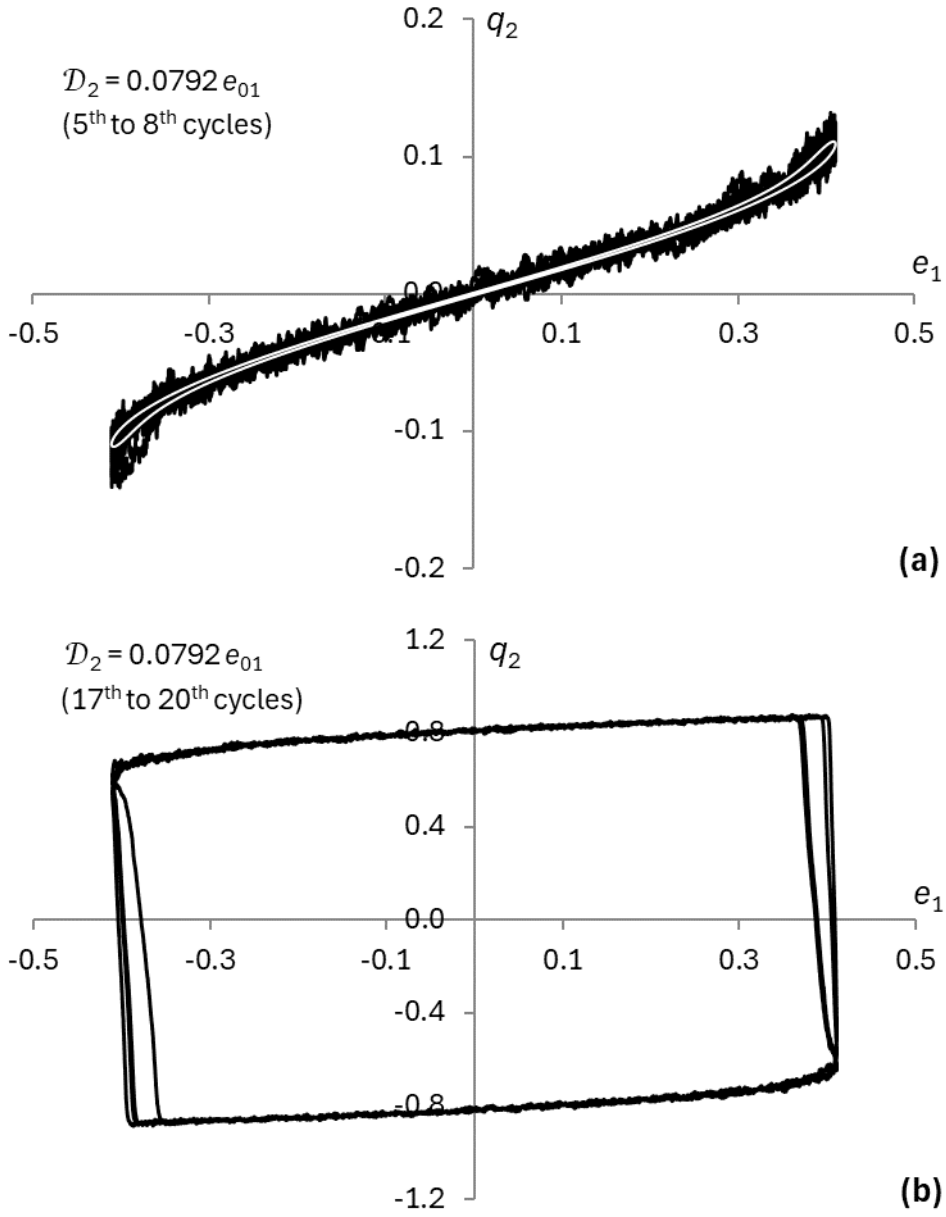

Fig. 4. (a) AFE hysteresis loops without noise (white loop, $\mathcal{D} = 0$) and AFE hysteresis loops with Gaussian white noise (black curves, $\mathcal{D}_2 = 0.0792e_{01}$) for the 5th to 8th cycles. (b) FE hysteresis loops induced by Gaussian white noise ($\mathcal{D}_2 = 0.0792e_{01}$) for the 17th to 20th cycles. Here, $f = f_1 = 0.5f_0$ and $|e_1| = e_{01} = 0.9857e_C$

When Gaussian white noise is activated, the transition from AFE hysteresis to FE hysteresis does not occur immediately but is delayed, as shown in the curves (s, q_1), (s, q_2) and (s, r_1), (s, r_2) in Figure 3. This is displayed as an abrupt change in the amplitudes of (s, q_1), (s, q_2) from less than 0.2 to greater than 0.6, and in (s, r_1), (s, r_2) from greater than 0.6 to approximately 0.0. For the noise amplitudes $\mathcal{D}_1 = 0.0630e_{01}$ and $\mathcal{D}_2 = 0.0792e_{01}$, the transitions from AFE hysteresis to FE hysteresis are delayed until the 23rd and 14th cycles, respectively. This indicates that a larger amplitude of Gaussian white noise results in a shorter delay time for the AFE to FE phase transition. The noise amplitude required to induce the transition is identified as $\mathcal{D}_3 = 0.0793e_{01}$, which is the smallest amplitude necessary to observe the transition occurring in the first cycle.

The numerical results indicate that when the amplitude of the field is smaller than the transition amplitude (i. e., $e_{01} < e_{0T1}$), and in the absence of noise ($\mathcal{D} = 0$), the system displays only the AFE hysteresis curve, depicted as a white loop in Figure 4(a). The black curves in Figures 4(a) and 4(b) show the hysteresis loops with Gaussian white noise, derived from a selected curve in Figure 3, specifically the (e_1, q_2) curve for $\mathcal{D}_2 = 0.0792e_0$, focusing on the 5th to 8th cycles (before the transition) and

the 17th to 20th cycles (after the transition), respectively. Due to the applied noise, the four successive AFE and FE hysteresis loops in Figures 4(a) and 4(b) show fluctuations and do not overlap. In particular, the black AFE hysteresis loops in Figure 4(a) exhibit fluctuations around the white loop. The FE hysteresis loops in Figure 4(b) exhibit both stable and unstable states, corresponding to the parts with positive and negative slopes.

The numerical results for the second set of frequency and amplitude, namely $f = f_2 = 1.5f_0$ and $|e_2| = e_{02} = 1.0443e_C$, with a standard deviation of $\sqrt{\Delta s_2} \approx 4.419086983258320 \times 10^{-2}$, are shown in Figures 5 and 6. In Figure 5, the time series curves display e_2 versus s (i. e., (s, e_2)), along with three q versus s curves (i. e., (s, q_4), (s, q_5), (s, q_6)), and three r versus s curves (i. e., (s, r_4), (s, r_5), (s, r_6)). These curves correspond to three amplitudes of noise: $\mathcal{D}_4 = 0.0561e_{02} = 0.05858523e_C$, $\mathcal{D}_5 = 0.0813e_{02} = 0.08490159e_C$, and $\mathcal{D}_6 = 0.0866e_{02} = 0.09043638e_C$. For all these curves, e_2 is switched on from the 1st to the 45th cycles and switched off after the 45th cycle, whereas noise is switched on from the 1st to the 35th cycles, and switched off after the 35th cycle.

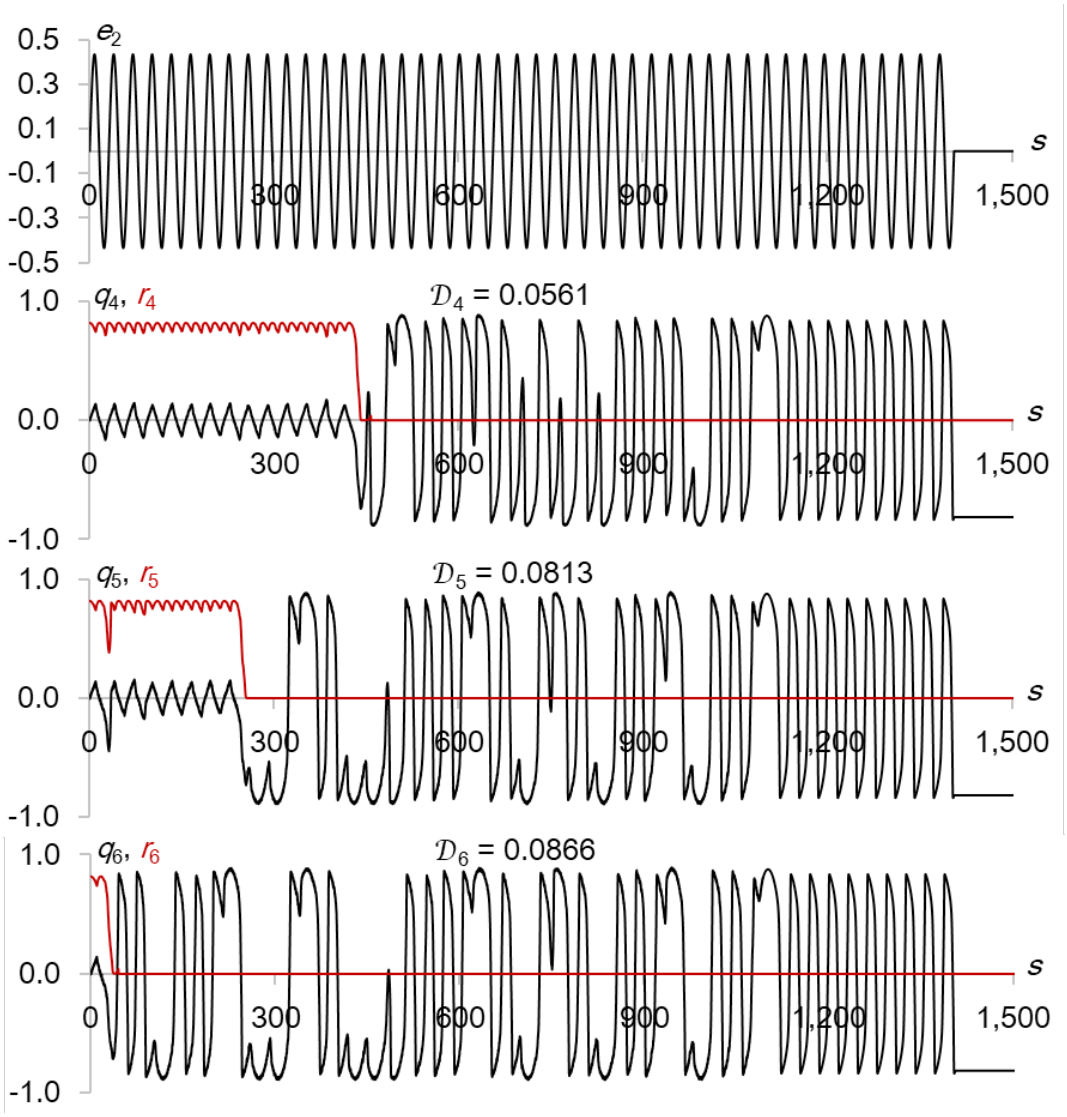

Fig. 5. Time series curves for (s, e_2), (s, q_4), (s, r_4), (s, q_5), (s, r_5), (s, q_6), and (s, r_6) for the 1st to 45th cycles. The three black (s, q) curves and three red (s, r) curves correspond to three amplitudes of noise: $\mathcal{D}_4 = 0.0561e_{02}$, $\mathcal{D}_5 = 0.0813e_{02}$, and $\mathcal{D}_6 = 0.0866e_{02}$. Here, $|e_2| = e_{02} = 1.0443e_C$, $f = f_2 = 1.5f_0$, and $\sqrt{\Delta s_2} \approx 4.419086983258320 \times 10^{-2}$; all noise is switched off after the 35th cycle

https://www.doi.org/10.33910/2687-153X-2025-6-1-35-48

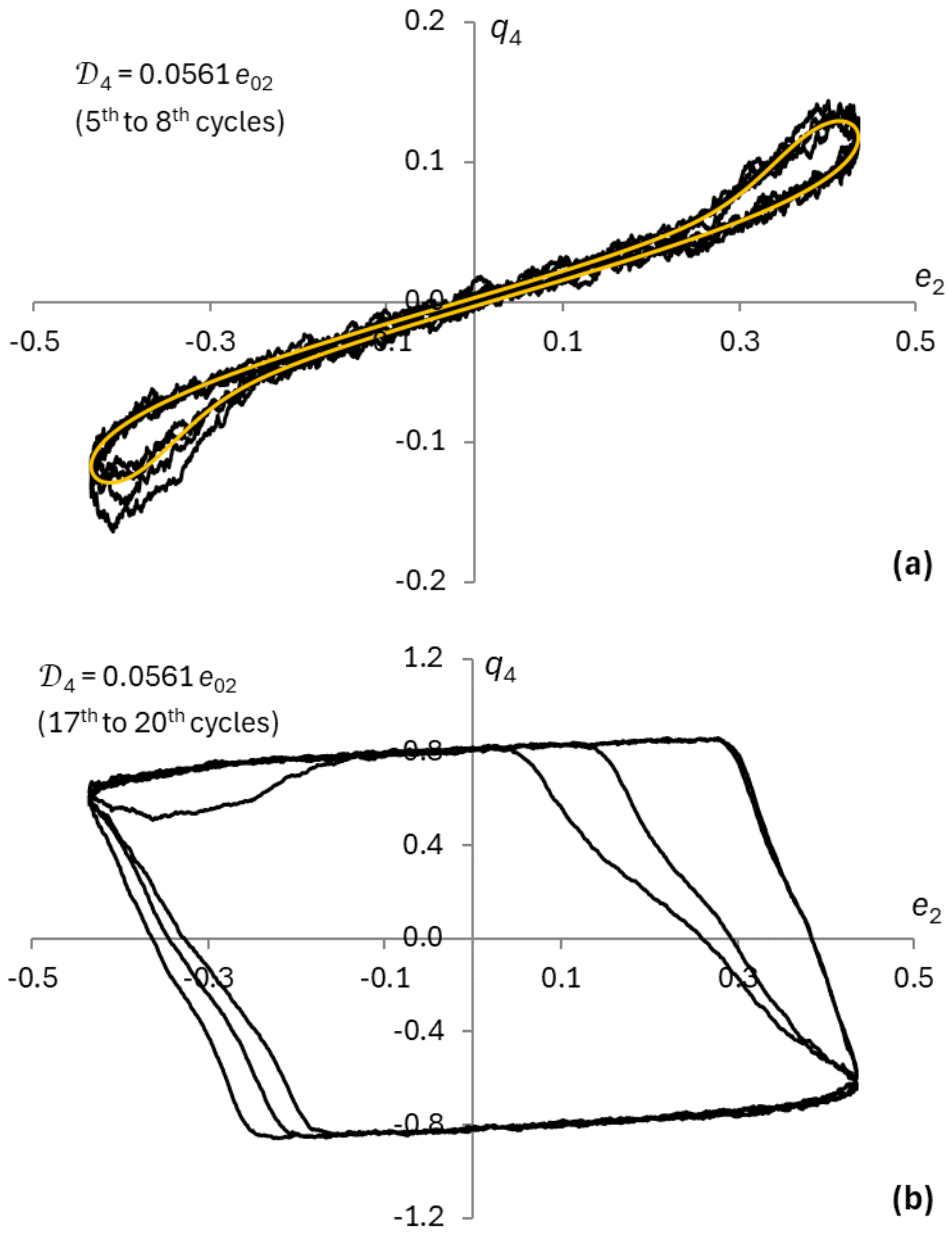

Fig. 6. (a) AFE hysteresis loops without noise (yellow loop, $\mathcal{D} = 0$) and AFE hysteresis loops with Gaussian white noise (black curves, $\mathcal{D}_4 = 0.0561e_{02}$) for the 5th to 8th cycles. (b) FE hysteresis loops induced by Gaussian white noise ($\mathcal{D}_4 = 0.0561e_{02}$) for the 17th to 20th cycles. Here, $f = f_2 = 1.5f_0$ and $e_0 = e_{02} = 0.9857e_C$

As with the first set of results, when Gaussian white noise is introduced, the transition from AFE to FE hysteresis does not occur immediately after noise is switched on; instead, it is delayed, as shown in the curves (s, q_4), (s, q_5) and (s, r_4), (s, r_5) in Figure 5. For the noise amplitudes $\mathcal{D}_4 = 0.0561e_{02}$ and $\mathcal{D}_5 = 0.0813e_{02}$, the transitions from AFE to FE hysteresis are delayed until the 14th and 8th cycles, respectively. This reflects the inversely proportional relationship between noise amplitude and time delay for the AFE to FE phase transition. The transition noise amplitude is identified as $\mathcal{D}_6 = 0.0866e_{02}$. In addition to the AFE to FE phase transitions, the three (s, q) curves in Figure 5 exhibit desynchronization, or phase slips, and a loss of periodicity while Gaussian white noise is switched on. The appearance of these features is the result of the crossing of unstable and fluctuating orbits (Berglund 2016).

When the amplitude of the field is smaller than the transition amplitude (i. e., $e_{02} < e_{0T2}$), and in the absence of noise ($\mathcal{D} = 0$), the system displays only the AFE hysteresis curve, depicted as a yellow loop in Figure 6(a). In contrast, the black curves in Figures 6(a) and 6(b) represent the hysteresis loops with Gaussian white noise, derived from the (e_2, q_4) curve in Figure 5, for $\mathcal{D}_4 = 0.0561e_{02}$, during the 5th to 8th cycles and the 17th to 20th cycles, corresponding to the periods before and after the AFE to FE phase

transition. As a result of the applied noise, the four successive AFE and FE hysteresis loops in Figures 6(a) and 6(b) do not overlap and show fluctuations. In particular, the black AFE curves in Figure 6(a) exhibit fluctuations around the yellow loop, while the FE hysteresis loops in Figure 6(b) display both stable and unstable states, corresponding to the parts with positive and negative slopes. The large and distorted deviations observed among the four successive FE hysteresis loops in Figure 6(b) are manifestations of desynchronization, or phase slips, as seen in the time series curve $(s, q)_4$ in Figure 5.

Part III: Hysteresis effects in the FE phase under strong field and moderate Gaussian white noise

In this section, the formalism, material parameters, and numerical schemes are the same as those in the second part. To enable comparison with the results from the second part, the same two frequencies and standard deviations are selected, i. e., $f_1 = 0.5f_0$ and $f_2 = 1.5f_0$. The selected strong field amplitudes for the two frequencies are $|e_3| = e_{03} = 1.5e_C$ and $|e_4| = e_{04} = 3.0e_C$, respectively, which are approximately 147.6% and 278.4% of the transition amplitudes e_{0T1} and e_{0T2}, respectively. To assess the effects of Gaussian white noise, moderate noise amplitudes of $\mathcal{D}_7 = 0.1e_{03} = 0.15e_C$ and $\mathcal{D}_8 = 0.1e_{04} = 0.30e_C$ are selected for the two frequencies, respectively. The numerical results for both frequencies, covering the 1st to 10th cycles, are presented in Figures 7 and 8.

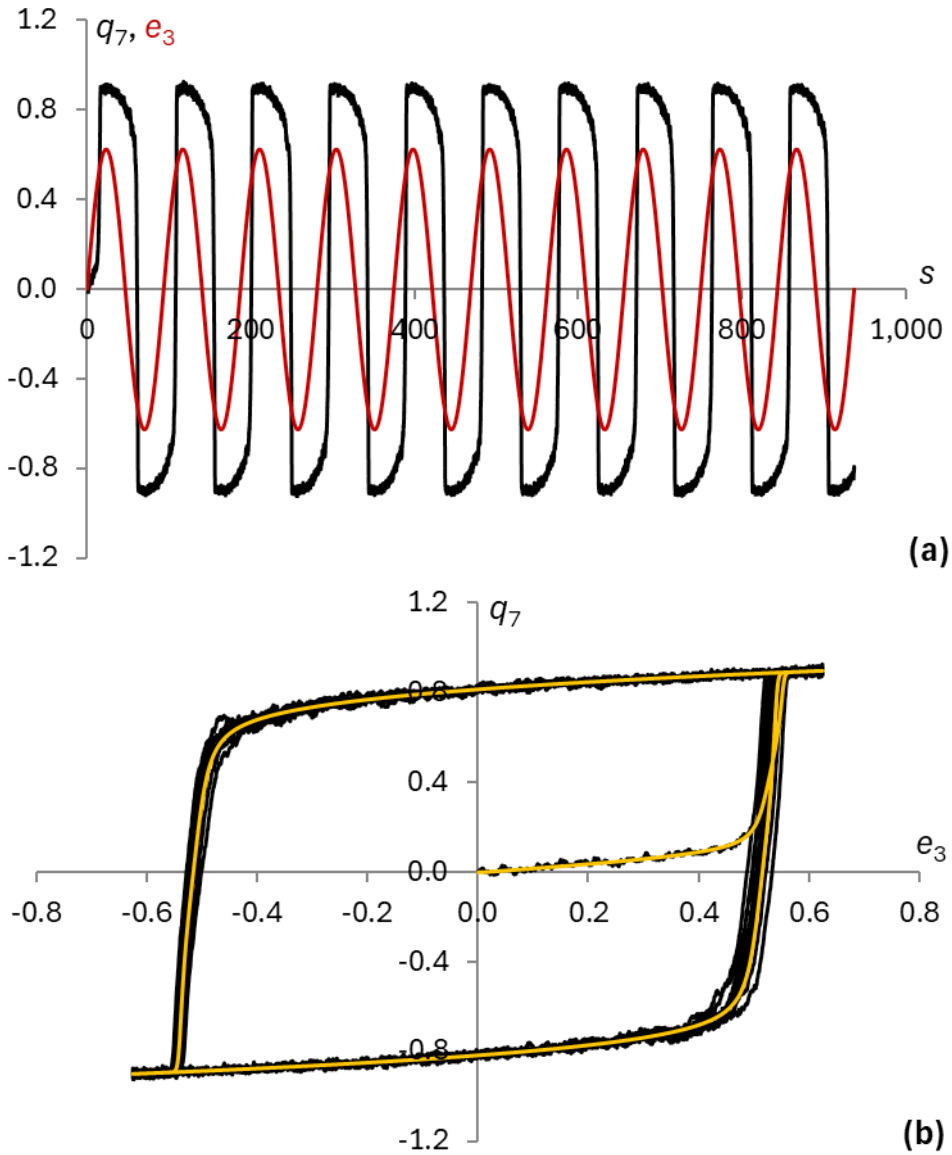

Fig. 7. (a) (s, e_3) and (s, q_7) time series curves. The (s, q_7) time series curve corresponds to Gaussian white noise with amplitude $\mathcal{D}_7 = 0.1e_{03}$. (b) FE hysteresis loops without noise (yellow loop, $\mathcal{D} = 0$), and FE hysteresis loops with Gaussian white noise, (e_3, q_7) (black curves, $\mathcal{D}_7 = 0.1e_{03}$), Here, $f = f_1 = 0.5f_0$, $|e_3| = e_{03} = 1.5e_C$, $\sqrt{\Delta s_1} \approx 7.654083178069687 \times 10^{-2}$, and the time range is 1st to 10th cycles

https://www.doi.org/10.33910/2687-153X-2025-6-1-35-48

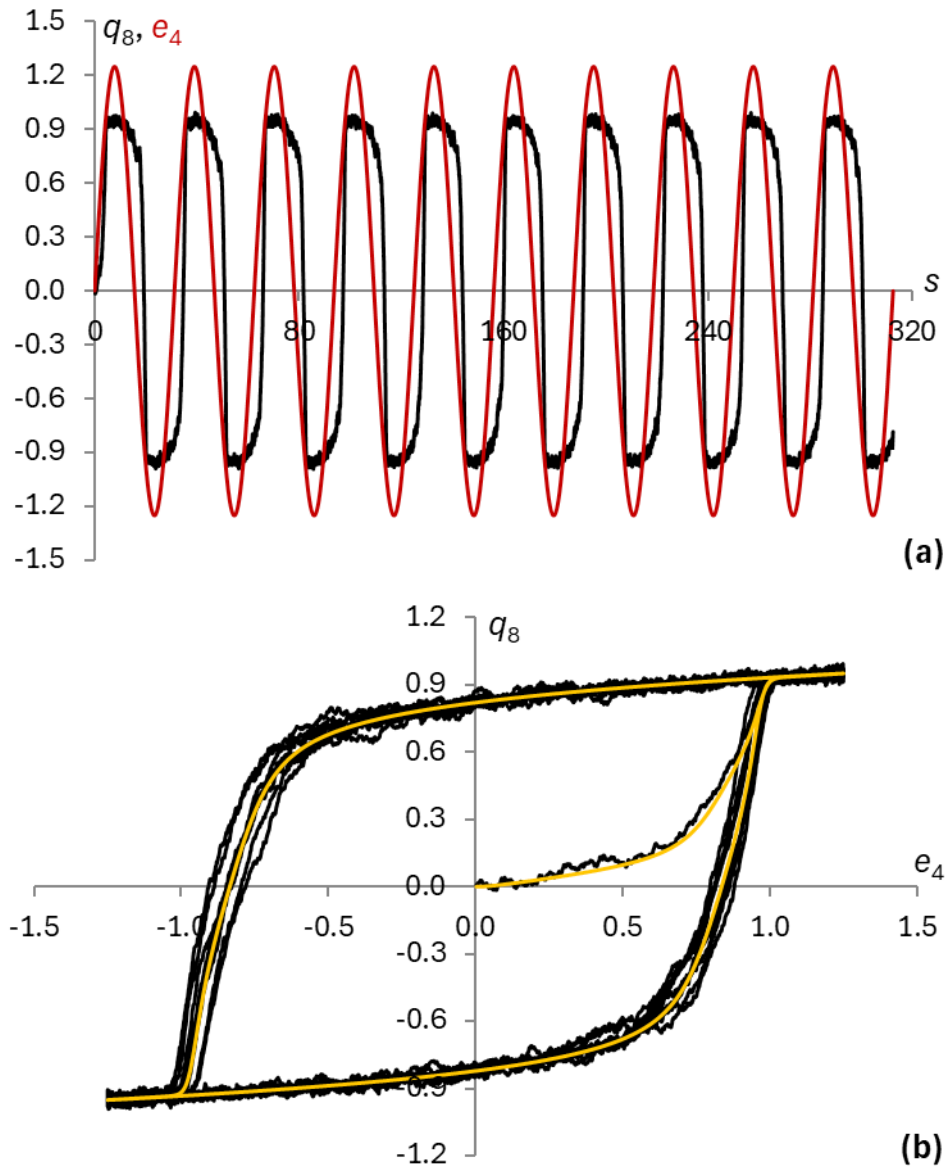

Fig. 8. (a) (s, e_4) and (s, q_8) time series curves. The (s, q_8) time series curve corresponds to Gaussian white noise with amplitude $\mathcal{D}_8 = 0.1e_{03}$. (b) FE hysteresis loops without noise (yellow loop, $\mathcal{D} = 0$), and FE hysteresis loops with Gaussian white noise (black curves, $\mathcal{D}_8 = 0.1e_{03}$), Here, $f = f_2 = 1.5f_0$, $|e_4| = e_{04} = 3.0e_C$, $\sqrt{\Delta s_2} \approx 4.419086983258320 \times 10^{-2}$, and the time range is 1st to 10th cycles

For f_1, the time series curves (s, e_3) and (s, q_7) are represented by the red and black curves in Figure 7(a). Similarly, for f_2, the time series curves (s, e_4) and (s, q_8) are represented by the red and black curves in Figure 8(a). The corresponding hysteresis curves (e_3, q_7) and (e_4, q_8) are shown in Figures 7(b) and 8(b). The numerical results indicate that in the absence of noise ($\mathcal{D} = 0$), the system shows only a single FE hysteresis loop, represented by the yellow hysteresis loop in Figures 7(b) and 8(b). Upon the introduction of Gaussian white noise, the FE hysteresis loops fluctuate around the yellow hysteresis loop and do not overlap. Given that the field amplitudes are significantly larger than the corresponding transition amplitudes e_{0T1} and e_{0T2}, the time series curves (s, q_7) and (s, q_8) in Figures 7(a) and 8(a) do not exhibit the pronounced desynchronization or phase slips, as seen in Figure 5.

Conclusions

The results in the first part of the reported study show the steady states of the selected AFE system, specifically ADP, under the applied static electric field. The numerical results demonstrate possible states of the system, including stable, unstable, and metastable states, as shown in Figure 1. By eliminating

unstable states and AFE states with $\bar{e} \geq e_C$, clear AFE and FE hysteresis patterns emerge, with the corresponding magnitudes of the induced normal electric displacement at $|q| < 0.2$ and $|q| > 0.6$, respectively. These steady states provide a baseline for identifying the AFE and FE phases in the second and third parts of the study.

In the second part, it is observed that for ADP, without the application of noise, a higher frequency requires a greater field amplitude for the dynamic phase transition from AFE to FE phases. For both selected frequencies, $f_1 = 0.5f_0 < f_0$ and $f_2 = 1.5f_0 > f_0$, and with the selected field amplitudes slightly below the critical field amplitudes (around 97%), additional Gaussian white noise with amplitudes less than 8% of the field amplitude induces a dynamic phase transition from AFE to FE phases. These phase transitions, however, are delayed for noise amplitudes below the corresponding critical values. The higher the level of noise, the shorter the delay time. This is due to the nonlinear nature of the system, where the system's states are affected by their history or past states over time. Consequently, the influence of noise accumulates until it reaches the threshold for the phase transition from AFE to FE phases. The stronger the noise, the faster the system gains the energy to cross the energy barrier and thus escape from AFE to FE states (Kramers 1940; Schüller et al. 2020; Tsimring, Pikovsky 2001). Notably, the transition delay means that when plotting the 2D hysteresis curves, both AFE and FE hysteresis loops may coexist if the AFE phase duration is not excluded from the analysis.

The hysteresis loops in the FE phase exhibit both stable and unstable states, identified by the positive and negative slopes of different parts of the hysteresis loop, as shown in Figures 4(b) and 6(b). More unstable features in the FE phase include desynchronization, phase slips, and loss of periodicity, which are clearly observed in the q versus s curves in Figure 5. It is also observed that, at higher frequency of the field, these instabilities become more pronounced. This is evident from comparing (i) the deviations of the four consecutive hysteresis loops in Figure 6(b), which are larger than those in Figure 4(b), and (ii) the more obvious desynchronization, phase slips, and loss of periodicity in the q versus s curves in Figure 5 compared to Figure 3. These instabilities arise because the selected field amplitudes are close to the transition amplitudes for the two selected frequencies.

When the field amplitude is well above the transition amplitude, it is evident that only the FE phase exists, and the effects of moderate Gaussian white noise diminish considerably. This is clearly observed in Figures 7(b) and 8(b) as the loss of negative slopes in the hysteresis loops, along with the recovery of synchronization, as evidenced by the time series curves in Figures 7(a) and 8(a). The residual effects of noise manifest as fluctuated and non-overlapping hysteresis loops.

In summary, when the field amplitude is just below the transition amplitude, the addition of Gaussian white noise will provide energy to the AFE system to overcome the energy barrier from AFE to FE phases, thereby inducing a transition. The transition does not occur immediately but is delayed for noise amplitudes slightly below than the critical value. Once the AFE system transitions to the FE phase, it remains in this phase, even when the noise and/or field are switched off. This indicates that the noise and field-induced phase transition from AFE to FE phases is irreversible, which is significantly different from the modeled non-stop transitions between ice ages and interglacials (Alexandrov et al. 2018; Benzi et al. 1981; Nicolis 1982). The bulk AFE model used in this study (Equation 4) does not include stress, strain, size effects, surface effects, or restoring forces that could pin the AFE states, which contributes to the irreversibility of the transition. In contrast, the phase transition from AFE to FE phases induced solely by a deterministic sinusoidal electric field, does not exhibit any delayed behavior.

To conclude, for the antiferroelectric system in its first-order phase, manipulating the frequency, the amplitudes of the applied field, and the levels of Gaussian white noise can control the timing of the AFE to FE phase transition. This feature may have applications in systems which require controllable switching time from small to large values of a physical quantity, corresponding to the AFE ($|q| < 0.2$) to FE ($|q| > 0.6$)phase transition. Moreover, this feature will provide direct observations of the system's order parameter behavior in its time series, similar to climate transitions over time. In future research, the analytical and numerical techniques developed here may be modified to enable the restoration of the AFE phase, and the study of noise-plus-field-induced phase transitions may be applied to other physical systems, such as antiferromagnets.

Conflict of Interest

The author declares that there is no conflict of interest, either existing or potential.

 https://www.doi.org/10.33910/2687-153X-2025-6-1-35-48

References

Alexandrov, D. V., Bashkirtseva, I. A., Ryashko, L. B. (2018) Noise-induced transitions and shifts in a climate–vegetation feedback model. *Royal Society Open Science*, 5 (4), article 171531. http://dx.doi.org/10.1098/rsos.171531 (In English)

Benzi, R., Sutera, A., Vulpiani, A. (1981) The mechanism of stochastic resonance. *Journal of Physics A: Mathematical and General*, 14 (11), L453–L457. https://doi.org/10.1088/0305-4470/14/11/006 (In English)

Berglund, N. (2016) Noise-induced phase slips, log-periodic oscillations, and the Gumbel distribution. *Markov Processes and Related Fields*, 22 (3), 467–505. https://hal.science/hal-00967427v2 (In English)

Cao, F. J., Wood, K., Lindenberg, K. (2007) Noise-induced phase transitions in field-dependent relaxational dynamics: The Gaussian ansatz. *Physical Review E*, 76 (5), article 051111. https://doi.org/10.1103/PhysRevE.76.051111 (In English)

Carrillo, O., Ibañes, M., García-Ojalvo, J. et al. (2003) Intrinsic noise-induced phase transitions: Beyond the noise interpretation. *Physical Review E*, 67 (4), article 046110. https://doi.org/10.1103/PhysRevE.67.046110 (In English)

Dagvadorj, G., Fellows, J. M., Matyjaśkiewicz, S. et al. (2015) Nonequilibrium phase transition in a two-dimensional driven open quantum system. *Physical Review X*, 5 (4), article 041028. https://doi.org/10.1103/PhysRevX.5.041028 (In English)

Garcia-Ojalvo, J., Sancho, J. M. (1999) *Noise in Spatially Extended Systems*. New York: Springer Publ., 307 p. (In English)

Gardiner, C. W. (1985) *Handbook of stochastic methods: For physics, chemistry and the natural sciences*. 2nd ed. Berlin: Springer Publ., 442 p. (In English)

Ghosh, P. K., Barik, D., Ray, D. S. (2005) Noise-induced transition in a quantum system. *Physics Letters A*, 342 (1–2), 12–21. https://doi.org/10.1016/j.physleta.2005.04.097 (In English)

Henkel, M., Pleimling, M. (2010) *Non-equilibrium phase transitions. Vol. 2: Ageing and dynamical scaling far from equilibrium*. Dordrecht: Springer Publ., 544 p. (In English)

Jin, Y., Xu, P. (2020) Noise-induced transitions and resonances in a delayed triple-well potential system. In: W. Lacarbonara, B. Balachandran, J. Ma et al. (eds.). *Nonlinear Dynamics of Structures, Systems and Devices: Proceedings of the First International Nonlinear Dynamics Conference (NODYCON 2019)*. Cham: Springer Publ., pp. 523–531. https://doi.org/10.1007/978-3-030-34713-0_52 (In English)

Khodabin, M., Rostami, M. (2015) Mean square numerical solution of stochastic differential equations by fourth order Runge-Kutta method and its application in the electric circuits with noise. *Advances in Difference Equations 2015*, 2015, article 62. https://doi.org/10.1186/s13662-015-0398-6 (In English)

Kramers, H. A. (1940) Brownian motion in a field of force and the diffusion model of chemical reactions. *Physica*, 7, 4, 284–304. https://doi.org/10.1016/S0031-8914(40)90098-2 (In English)

Levkivskyi, I. P., Sukhorukov, E. V. (2009) Noise-induced phase transition in the electronic Mach-Zehnder interferometer. *Physical Review Letters*, 103, article 036801. https://doi.org/10.1103/PhysRevLett.103.036801 (In English)

Lim, S.-Ch. (2022) Numerical simulations of nonlinear and chaotic order parameter responses in bulk antiferroelectrics using ammonium dihydrogen phosphate parameter. *Physics of Complex Systems*, 3 (3), 122–136. https://www.doi.org/10.33910/2687-153X-2022-3-3-122-136 (In English)

Lim, S.-Ch. (2023) Calculations of Lyapunov exponents and characterizations of nonlinear dynamics in bulk antiferroelectrics. *Physics of Complex Systems*, 4 (4), 176–194. https://www.doi.org/10.33910/2687-153X-2023-4-4-176-194 (In English)

Lines, M. E., Glass, A. M. (1977) *Principles and applications of ferroelectrics and related materials*. Oxford: Oxford University Press, 664 p. (In English)

Liu, S., Li, M.-R., Zhang, S.-Z. et al. (2024) Noise-induced phase transitions in hybrid quantum circuits. *Physical Review B*, 110 (6), article 064323. https://doi.org/10.1103/PhysRevB.110.064323 (In English)

Nicolis, C. (1982) Stochastic aspects of climatic transitions-response to a periodic forcing. *Tellus*, 34 (1), 1–9. https://doi.org/10.3402/tellusa.v34i1.10781 (In English)

Press, W. H., Teukolsky, S. A., Vetterling, W. T., Flannery, B. P. (1996) *Numerical Recipes in C: The Art of Scientific Computing*. 2nd ed. Cambridge: Cambridge University Press, 537 p. (In English)

Schüller, B., Meistrenko, A., van Hees, H. et al. (2020) Kramers' escape rate problem within a non-Markovian description. *Annals of Physics*, 412, article 168045. https://doi.org/10.1016/j.aop.2019.168045 (In English)

Tolédano, P., Guennou, M. (2016) Theory of antiferroelectric phase transitions. *Physical Review B*, 94 (1), article 014107. https://doi.org/10.1103/PhysRevB.94.014107 (In English)

Tong, N. H., Vojta, M. (2006) Signatures of a noise-induced quantum phase transition in a mesoscopic metal ring. *Physical Review Letters*, 97 (1), article 016802. https://doi.org/10.1103/PhysRevLett.97.016802 (In English)

Tsimring, L. S., A. Pikovsky, A. (2001) Noise-induced dynamics in bistable systems with delay. *Physical Review Letters*, 87 (25), article 250602. https://doi.org/10.1103/PhysRevLett.87.250602 (In English)

Van den Broeck, C., Parrondo, J. M. R., Toral, R. (1994) Noise-induced nonequilibrium phase transition. *Physical Review Letters*. 73 (25), 3395–3398. https://doi.org/10.1103/PhysRevLett.73.3395 (In English)

Zhang, G., Novais, E., Baranger, H. U. (2017) Rescuing a quantum phase transition with quantum noise. *Physical Review Letters*, 118 (5), article 050402. https://doi.org/10.1103/PhysRevLett.118.050402 (In English)

Zhang, M.-H., Fulanović, L., Egert, S. et al. (2020) Electric-field-induced antiferroelectric to ferroelectric phase transition in polycrystalline NaNbO3. *Acta Materialia*, 200, 127–135. https://doi.org/10.1016/j.actamat.2020.09.002 (In English)

Zhang, M.-H., Fulanović, L., Zhao, C. H., Koruza, J. (2023) Review on field-induced phase transitions in lead-free NaNbO3-based antiferroelectric perovskite oxides for energy storage. *Journal of Materiomics*, 9 (1), 1–18. https://doi.org/10.1016/j.jmat.2022.09.008 (In English)